



Cite this: *Sustainable Energy Fuels*, 2025, **9**, 5882

## Enhancing air-cathode MFC performance using bio-palladium catalysts and microbial consortia

Khanyisile B. Malunga-Makatu, \* Shepherd M. Tichapondwa and Evans M. N. Chirwa

Air-cathode microbial fuel cells (MFCs) offer a sustainable approach to bioelectricity generation, but their commercialization is hindered by costly platinum catalysts and inefficient microbial electron transfer. This study investigates bio-palladium (bio-Pd) nanoparticles as a cost-effective cathode catalyst and optimizes microbial consortia to enhance MFC performance. Four cathode configurations were tested, two incorporating bio-Pd (9.6–16.9 nm, characterized via XRD and SEM-EDS), alongside sulfate-reducing bacteria (SRB) and marine bacteria (MB) cultures. The CM3 cathode, combining bio-Pd, activated charcoal, and carbon black, achieved a peak power density of  $3.70 \pm 0.15 \text{ mW m}^{-2}$ , six times higher than the control, with a low internal resistance of  $210 \pm 15 \Omega \text{ m}^2$ . MB, dominated by electroactive *Paraclostridium* sp., outperformed SRB, delivering  $4.18 \pm 0.17 \text{ mW m}^{-2}$  due to its dense biofilm (85% anode coverage) and efficient direct and indirect electron transfer, as confirmed by 16S rRNA sequencing and SEM. These advancements, yielding power densities comparable to bio-catalytic systems, highlight bio-Pd's potential as a sustainable alternative to platinum and *Paraclostridium*'s role as a high-performance inoculum. Addressing South Africa's energy challenges and UN Sustainable Development Goals (6, 7, 9, 13), this work paves the way for scalable MFCs in wastewater treatment and renewable energy, though long-term stability requires further exploration.

Received 9th May 2025  
Accepted 12th September 2025

DOI: 10.1039/d5se00664c  
[rsc.li/sustainable-energy](http://rsc.li/sustainable-energy)

## 1 Introduction

Microbial fuel cells (MFCs) represent a promising technology for sustainable energy production, converting the chemical energy of organic substrates directly into electrical energy through the metabolic activity of electroactive microorganisms.<sup>1</sup> This dual-purpose capability, simultaneous wastewater treatment and bioelectricity generation, positions MFCs as a pivotal innovation in the global transition towards cleaner energy systems. The urgency of this transition is underscored by ongoing energy insecurity, exemplified by South Africa's extensive load-shedding events in 2022, which totalled over 200 days.<sup>2</sup> MFCs, therefore, offer a potential pathway toward addressing these challenges while supporting several United Nations Sustainable Development Goals (SDGs), including SDG 6 (Clean Water and Sanitation), SDG 7 (Affordable and Clean Energy), SDG 9 (Industry, Innovation, and Infrastructure), and SDG 13 (Climate Action).<sup>3</sup>

Despite their potential, the practical deployment of MFCs remains constrained by several technical challenges, primarily related to current instability, high internal resistance, biofilm inefficiencies, biofouling of membranes and electrodes,<sup>4</sup> low

power output, catalyst durability, and material costs<sup>5</sup> among other operational issues. To overcome these barriers, research has focused on advances in microbial community engineering, electrodes materials, reactor design, biofilm control and membrane technologies. Engineered strains such as *Shewanella oneidensis* and synthetic microbial consortia have enhanced extracellular electron transfer, broadened substrate use, and improved simultaneous power generation and pollutant degradation.<sup>6</sup> Electrode innovations, including nanomaterials (e.g., platinum and palladium nanoparticles, graphene oxide) and bio-derived carbons, have increased surface area, conductivity, and catalytic activity while low-cost metal oxide composites address fabrication expenses.<sup>7</sup> Meanwhile, biofilm management through surface modifications, and enzymatic approaches, reduces biofouling and enhances stability.<sup>8</sup>

While these strategies have improved microbial activity, substrate utilization, and overall system stability, a critical aspect of further advancing MFC technology lies in enhancing the electrochemical performance of electrode materials, especially the cathode, which governs the oxygen reduction reaction (ORR), the rate-limiting step in many MFC systems.<sup>9</sup> The efficacy of ORR depends significantly on the surface properties, electrical conductivity, chemical stability, and catalytic activity of the cathode material. Conventionally, platinum-based catalysts have been used for their superior activity; however, their high cost and poor long-term stability necessitate the

Water Utilisation and Environmental Engineering Division, Department of Chemical Engineering, University of Pretoria, Pretoria 0002, South Africa. E-mail: kb.malunga-makatu@tuks.co.za



development of alternative, more sustainable options.<sup>10</sup> Recent advancements have explored the application of transition metals, carbonaceous composites, and biocatalytic materials as viable substitutes.<sup>11</sup>

Among these, biocatalytic cathode materials comprising microorganisms, enzymes, or biologically derived nanoparticles, have gained increasing attention due to their ecological compatibility, cost-effectiveness, and resistance to biofouling.<sup>10</sup> The catalytic properties of biocatalytic materials were first identified in a 1997 study on seawater batteries; the study demonstrated that microbial biofilms could enhance cathodic performance in seawater batteries by facilitating ORR, although excessive biofilm growth was shown to hinder oxygen diffusion.<sup>12</sup>

Recent advancements in biocatalytic reactions have highlighted significant potential for improving the efficiency and sustainability of electrochemical systems. A particularly promising avenue involves the microbial synthesis of metal nanoparticles such as platinum and palladium (bio-Pt and bio-Pd), which combine high catalytic activity with improved operational durability.<sup>13</sup> Bio-Pd, in particular, has demonstrated electrocatalytic capabilities comparable to chemically synthesized analogues.<sup>14</sup> For instance, Pd nanoparticles produced by *Shewanella oneidensis* MR-1 have been shown to enhance hydrogen deposition on carbon nanotube supports.<sup>15</sup> While *Citrobacter* sp. derived bio-Pd has been used to improve anode electrocatalytic activity in MFCs.<sup>16</sup> Despite the above advances, the application of bio-Pd as a catalyst for the cathode remains largely unexplored.

In parallel to advancements in catalyst design, microbial community composition at the anode has emerged as a key determinant of MFC performance. The optimization of microbial consortia can enhance extracellular electron transfer (EET) either through direct contact with the electrode or *via* soluble electron shuttles.<sup>1</sup> Marine and sulfate-reducing bacteria, for example, are known to exhibit varying degrees of electroactivity, which may influence power output depending on environmental conditions and substrate availability. Marine bacteria, especially marine actinobacteria and specific species like *Pseudoalteromonas* and *Phaeobacter*, have natural antifouling properties. These bacteria produce compounds that inhibit biofilm formation by unwanted fouling microbes on surfaces like stainless steel or membranes, reduces maintenance without harmful chemical, mitigating membrane fouling which is a major challenge for long-term MFC operation.<sup>17</sup> They form biofilms compatible with electrodes, supporting stable microbial communities, extracellular electron transfer, and resilient power generation. Their adaptability to saline environments and production of extracellular polymeric substances (EPS) further broaden MFC applications while improving efficiency and long-term stability.<sup>18</sup> Sulfate-reducing bacteria enhance MFC performance by coupling sulfate reduction with renewable energy generation, including hydrogen and methane, while simultaneously supporting stable extracellular electron transfer (EET).<sup>19</sup> They enable efficient chemical oxygen demand (COD) and sulfate removal under moderate conditions with low sludge production, making them cost-effective for large-scale

applications. Their robust biofilms and flexible EET mechanisms further improve system stability and adaptability for treating sulfate-rich wastewaters.<sup>20</sup> Nevertheless, successful real-world application will require optimization of reactor design, electrode configuration, and long-term microbial community stability to ensure reliable performance under variable environmental conditions.

This study aims to investigate the synergistic effects of cathode material modification and microbial community composition on the performance of an air-cathode MFC. Specifically, it evaluates the impact of bio-Pd integrated with activated carbon and carbon black as cathode catalysts and compares the electrogenic potential of two distinct microbial cultures: sulfate-reducing bacteria (SRB) and marine bacteria (MB). The overarching objective is to enhance the power density and operational stability of MFCs, thereby advancing their feasibility for real-world energy and wastewater treatment applications.

## 2 Materials and method

This study was conducted in two phases to evaluate the performance of air-cathode microbial fuel cells (MFCs). Phase 1 focused on the integration of bio-palladium (bio-Pd) nanoparticles as a cathode catalyst, while Phase 2 assessed the influence of two microbial cultures on MFC performance. All experiments were performed under controlled conditions, with detailed protocols to ensure reproducibility.

### 2.1 Phase 1: bio-Pd catalysed air cathode

**2.1.1 Cathode and anode preparation.** Bio-Pd nanoparticles were synthesized using sulfate-reducing bacteria (SRB) following the method of Malunga and Chirwa.<sup>21</sup> SRB cells were harvested at mid-log phase and resuspended in a 100 mL buffer containing 1000 mg of  $\text{PdCl}_2$  (Merck, Gauteng, South Africa) and 25 mM sodium formate as the electron donor. The suspension, with an optical density ( $\text{OD}_{600}$ ) of 2.051, was adjusted to pH 6.0 using HCl and NaOH (Glass-world, Gauteng, South Africa). The solution was sparged with nitrogen for 6 minutes to create an anaerobic headspace, incubated at 35 °C with 110 rpm shaking for 6 hours, and then sparged with air to halt reduction. The resulting bio-Pd was centrifuged at 5000 rpm for 5 minutes at 10 °C, air-dried for 24 hours, and stored at 4 °C. Four cathode types (25  $\text{cm}^2$  each) were prepared using carbon mesh (Fuel Cell Store, USA): CM1: coated with a paste of 6 mg bio-Pd and 28 mg activated charcoal powder (ACP; Sigma-Aldrich, South Africa) mixed with polyvinylidene fluoride (PVDF; Sigma-Aldrich) as a binder. CM2: coated with 0.3 g ACP and 0.03 g carbon black (Vulcan XC-72, Cabot Corporation) in PVDF, following Mattsena *et al.*<sup>16</sup> CM3: coated with 0.3 g ACP, 0.03 g carbon black, and 6 mg bio-Pd in PVDF. CM4: unmodified carbon mesh (control). The anode was constructed from 25  $\text{cm}^2$  carbon mesh, folded and sewn to encase 2.0 g granulated activated carbon (particle size 0.60–1.1 mm; Sigma-Aldrich). All electrodes were sterilized by autoclaving at 121 °C for 15 minutes before assembly.



**2.1.2 Characterisation of bio-Pd cathode material.** Bio-Pd cathodes were characterized to confirm nanoparticle composition and morphology. Scanning electron microscopy (SEM) coupled with energy-dispersive X-ray spectroscopy (EDS) was performed using a Zeiss Ultra Plus Field Emission SEM (Zeiss, Germany) at 2 kV for imaging and 1.5 kV for EDS analysis. Samples were mounted on adhesive carbon tape on aluminium stubs and analysed using Oxford Instruments Aztec 3.0 SP1 software. X-ray diffraction (XRD) was conducted to identify crystalline phases and determine bio-Pd nanoparticle size, following Matsena *et al.*<sup>16</sup> XRD patterns were analysed using a Bruker D8 Advance diffractometer with Cu K $\alpha$  radiation ( $\lambda = 1.5406 \text{ \AA}$ ). Crystallite size was calculated using the Scherrer equation:

$$t = \frac{K\lambda}{\beta \cos \theta_\beta} \quad (1)$$

where  $t$  is the crystallite size (nm),  $K$  is the shape factor (0.9),  $\lambda$  is the X-ray wavelength,  $\beta$  is the full width at half maximum (FWHM) in radians, and  $\theta$  is the Bragg angle (degrees).

**2.1.3 Microbial fuel cell reactor set-up: cathode evaluation.** The MFC reactor consisted of a 320 mL anode chamber separated from the air-cathode by a Nafion 117 proton exchange membrane (Fuel Cell Store, USA). A 10 mL aliquot of actively growing SRB culture ( $\text{OD}_{600} \approx 1.0$ ) was inoculated into 310 mL of Postgate medium C (pH 7.0). The anode chamber was sparged with oxygen-free nitrogen for 3 minutes and sealed with butyl rubber stoppers to maintain anaerobic conditions. The four cathode types (CM1–CM4) were tested individually. Experiments were conducted at 35 °C with constant stirring at 120 rpm for 48 hours. Voltage output was monitored using a Uni-T UT61C multimeter (Uni-Trend Technology, Hong Kong) connected to a data acquisition system.

## 2.2 Phase 2: effect of microbial culture on MFC performance

### 2.2.1 Microbial culture preparation

*Sulfate-reducing bacteria (SRB).* SRB were isolated from sludge samples collected at the Brits Wastewater Treatment Plant, Northwest, South Africa, following ethical sampling guidelines. Cultures were grown in Postgate Medium C (pH 7.0) under anaerobic conditions, as described by Molokwane and Chirwa.<sup>22</sup> For experiments, 10 mL of mid-log phase SRB ( $\text{OD}_{600} \approx 1.0$ ) was inoculated into 90 mL of fresh Postgate Medium C and incubated at 35 °C for 48 hours in sealed serum bottles sparged with nitrogen and maintained under anaerobic conditions in sealed bottles.

*Marine bacteria (MB).* MB were isolated from estuarine sediment samples collected at Lagoon Beach, Cape Town, South Africa, with appropriate permits. Cultures were enriched in mineral salt medium (MSM; pH 7.2) by inoculating 10 mL of sediment water into 90 mL of MSM. The mixture was incubated anaerobically at 30 °C for 48 hours<sup>23</sup> after nitrogen sparging. Bacterial growth was confirmed by measuring  $\text{OD}_{600}$  using a WPA Lightwave II spectrophotometer (Biochrome, UK).

**2.2.2 Anodic microbial culture characterization.** Microbial cultures were characterized using 16S rRNA sequencing to identify electrogenic strains. SRB and MB were grown on Postgate Medium C and MSM agar plates, respectively, using the streak

plate method and incubated in an anaerobic chamber at 35 °C and 30 °C respectively for 5 days. Samples were sent to Inqaba Biotechnical Industries (Pty) Ltd (Gauteng, South Africa) for sequencing. Full-length 16S rRNA gene amplicons were sequenced on the PacBio Sequel system (Pacific Biosciences, USA). Raw sub-reads were processed using the SmartLink (v11.0) Circular Consensus Sequences algorithm to generate high accuracy reads (>QV40), followed by taxonomic analysis using vsearch and QIIME2. Anode morphology was analysed by SEM, with samples air-dried, mounted on carbon tape on aluminium stubs, and imaged at 2 kV using a Zeiss Ultra Plus Field Emission SEM.

**2.2.3 Microbial fuel cell reactor set-up: microbial culture evaluation.** The MFC setup mirrored that of Phase 1, with the CM3 cathode (0.3 g ACP, 0.03 g carbon black, 6 mg bio-Pd) used consistently to isolate the effect of microbial cultures. Two conditions were tested: (1) 10 mL of SRB inoculated into 310 mL of Postgate Medium C, and (2) 10 mL of MB inoculated into 310 mL of MSM. The anode chamber was sparged with nitrogen, sealed, and maintained at 35 °C and 30 °C respectively with 120 rpm stirring for 48 hours. Voltage output was recorded as described in Section 2.1.3.

## 2.3 Microbial fuel cell performance analysis

MFC performance was evaluated by measuring voltage across variable external resistances (1 k $\Omega$  to 560 k $\Omega$ ) after 24 h of incubation. Polarization curves were constructed, and current density ( $I$ , mA m $^{-2}$ ) was calculated following the method described by Logan.<sup>24</sup>

$$I = \frac{V}{R_{\text{ext}}A} \quad (2)$$

where  $V$  is the voltage (mV),  $A$  is the cathode area (m $^2$ ), and  $R_{\text{ext}}$  is the external resistance ( $\Omega$ ). Power density ( $P$ , mW m $^{-2}$ ) was determined as:

$$P = \frac{V^2}{R_{\text{ext}}A} \quad (3)$$

Internal resistant ( $R_{\text{int}}$ ,  $\Omega$  m $^2$ ) was derived from the polarization curve slope:

$$R_{\text{int}} = \frac{\Delta V}{\Delta I \times A} \quad (4)$$

where  $\Delta V$  is the change in voltage (V), and  $\Delta I$  is the change in current density (mA m $^{-2}$ ). Maximum power density ( $P_{\text{max}}$ , mW m $^{-2}$ ) was calculated as:

$$P_{\text{max}} = \frac{(\text{OCV})^2 R_{\text{ext}}}{(R_{\text{int}} + R_{\text{ext}})^2} \times \frac{1}{A} \times 10^3 \quad (5)$$

where OCV is the open circuit voltage (V). All measurements were performed in triplicates with mean values reported.

## 3 Results and discussion

### 3.1 Characterisation of bio-Pd cathode material

Four cathode types were evaluated: carbon mesh coated with bio-palladium and activated charcoal powder (CM1), carbon



mesh with activated charcoal powder and carbon black (CM2), carbon mesh with bio-palladium, activated charcoal powder, and carbon black (CM3), and unmodified carbon mesh (CM4, control). Prior to MFC testing, the bio-Pd nanoparticles were characterized to confirm their synthesis, composition, and morphology, as these properties critically influence oxygen reduction reaction (ORR) efficiency.

XRD patterns of bio-Pd samples exhibited distinct peaks at  $2\theta$  values of  $40.1^\circ$ ,  $46.7^\circ$ , and  $68.1^\circ$ , corresponding to the (111), (200), and (220) planes of face-centered cubic (FCC) palladium (JCPDS 46-1043), confirming successful microbial synthesis (Fig. 1). No impurity peaks (e.g., PdO) were detected, indicating high phase purity. Crystallite size, calculated using the Scherrer

equation, ranged from 9.6 to 16.9 nm, with an average of  $12.4 \pm 2.1$  nm ( $n = 3$ ). This nanoscale size is advantageous, as smaller particles provide a higher surface area-to-volume ratio, enhancing catalytic activity.<sup>25</sup> Compared to chemically synthesized Pd ( $\sim 20$ – $50$  nm), bio-Pd's smaller size aligns with findings by Redwood *et al.*<sup>26</sup> who reported 5–10 nm bio-Pd clusters with superior catalytic performance due to increased active sites. Similarly, Somorjai and Rioux<sup>27</sup> emphasized that precise particle size control at the molecular level is critical for achieving catalyst selectivity and activity. Nanoparticles within the range of 1–20 nm possess a high surface-to-volume ratio, thereby increasing the number of accessible active sites for catalytic reactions. In agreement, Matsena *et al.*<sup>16</sup> demonstrated that bio-Pd(0) nanoparticles sized 11.37 and 15.65 nm, synthesized using *Citrobacter* sp., significantly improved microbial fuel cell (MFC) performance. These small-sized Pd nanoparticles provided a catalytically active surface that facilitated electron transfer and catalyzed formate oxidation at the anode.

SEM analysis revealed distinct surface morphologies across the cathodes. The carbon mesh (Fig. 2A) showed smooth, aligned fibres with limited roughness, offering few active sites for catalysis and resulting in low power output. With the incorporation of activated charcoal (Fig. 2B–D), the electrode surface became more heterogeneous and porous, forming a high-surface-area matrix favourable for oxygen reduction reactions. As a result, cathodes CM1–CM3 exhibited higher power outputs (Fig. 3). Although no significant morphological differences were observed among CM1–CM3, variations in microbial fuel cell (MFC) performance were evident. The addition of bio-Pd to CM1 and CM3, confirmed by EDS mapping (Fig. 2E and F), enhanced catalytic activity by introducing discrete, well-dispersed active sites for oxygen reduction. As

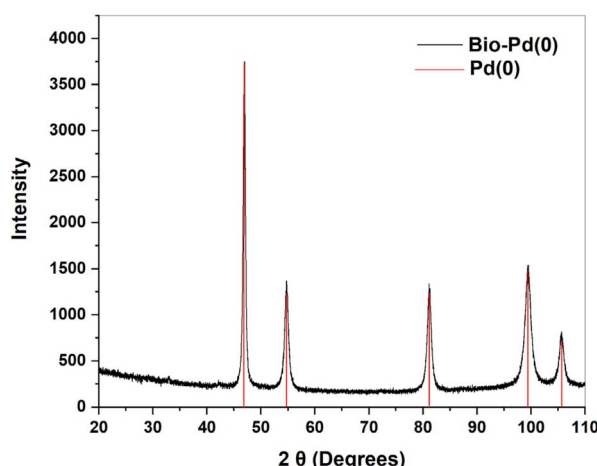


Fig. 1 XRD graph showing clearly defined peaks of bio-Pd that correspond to Pd(0) peaks.

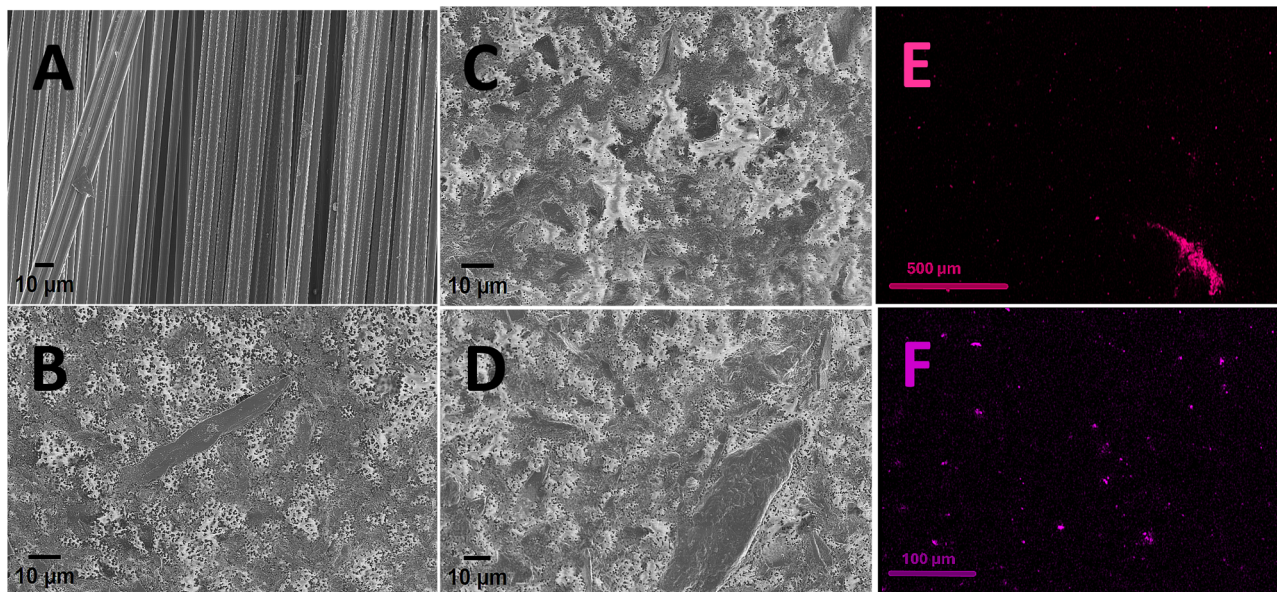


Fig. 2 SEM images of: (A) carbon mesh (CM 4); (B) carbon mesh, ACP, and CB (CM2); (C) carbon mesh, ACP and bio-Pd (CM 1); (D) carbon mesh, ACP, CB and bio-Pd (CM 3). EDS mapping of Pd on: (E) carbon mesh, ACP and bio-Pd (CM 1); (F) carbon mesh, ACP, CB and bio-Pd (CM 3).



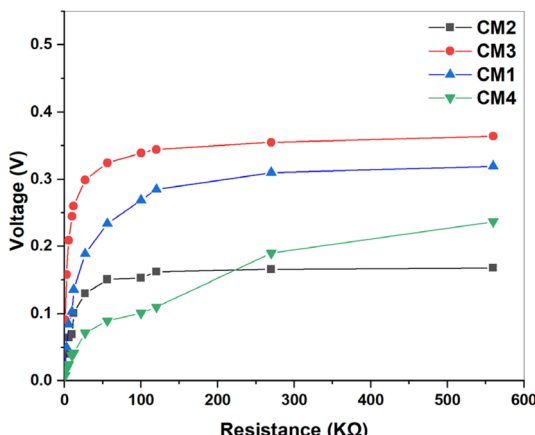


Fig. 3 Voltage vs. resistance curves for four MFC configurations; carbon mesh 1 (CM1) with bio-Pd and ACP, carbon mesh 2 (CM2) with ACP and carbon black, carbon mesh 3 (CM3) with bio-Pd, ACP and carbon black, and carbon mesh 4 (CM4) unmodified.

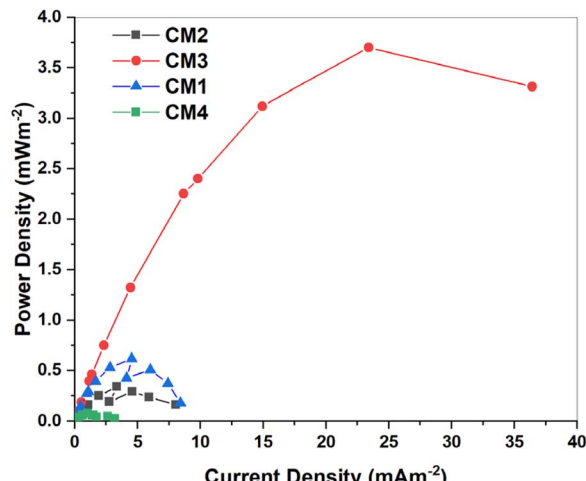


Fig. 5 Power density curves of an air-cathode MFC with four types of cathodes. Carbon mesh 1 (CM1) with bio-Pd and ACP, carbon mesh 2 (CM2) with ACP and carbon black, carbon mesh 3 (CM3) with bio-Pd, ACP and carbon black, and carbon mesh 4 (CM4) unmodified.

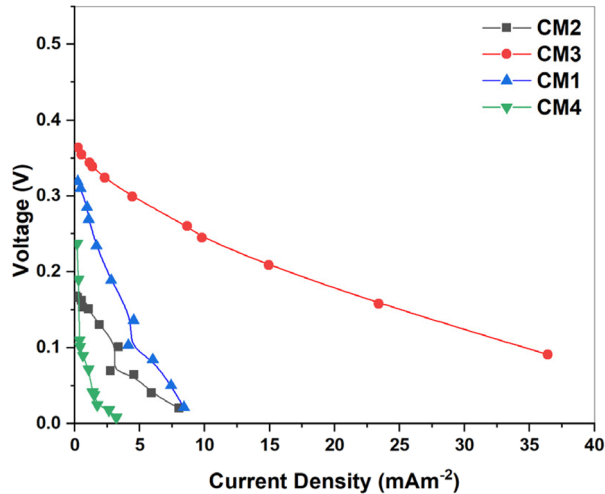


Fig. 4 Polarisation curves of an air-cathode MFC with four types of cathodes. Carbon mesh 1 (CM1) with bio-Pd and ACP, carbon mesh 2 (CM2) with ACP and carbon black, carbon mesh 3 (CM3) with bio-Pd, ACP and carbon black, and carbon mesh 4 (CM4) unmodified.

shown in Fig. 3–5, these two cathodes achieved the highest power densities, with CM3 outperforming all others, an improvement attributed to the synergistic effect of carbon black, activated carbon and bio-Pd.

Although direct quantification of the individual contributions of activated charcoal, carbon black, and bio-Pd was not performed in this study, according to the literature activated carbon serves as the primary catalyst for oxygen reduction at the cathode, offering high surface area, strong catalytic activity, environmental sustainability, and cost-effectiveness.<sup>28</sup> Its performance is further enhanced when blended with carbon black (CB), which increases electrical conductivity, facilitates faster electron transfer during the oxygen reduction reaction (ORR), and reduces charge transfer resistance, thereby improving limiting current, power density, and long-term

stability, particularly at optimal ratios of ~10%.<sup>28</sup> In addition, bio-Pd nanoparticles act as a catalyst that further enhances catalytic activity especially when combined or hybridized with conductive supports such as carbon nanotubes or doped bio-carbon, the catalytic activity further improves due to enhanced electron conduction pathways, increasing effective active surface sites, improving overall cell potential, and boosting power output.<sup>15</sup> The synergistic interaction of these three components resulted in the superior electrochemical performance observed for CM3.

The characterization results validate the successful integration of bio-Pd nanoparticles into the cathode matrix, particularly for electroactive surface area compared to commercial Pd catalysts, as reported by Quan *et al.*,<sup>29</sup> who noted that Pd nanoparticles below 20 nm significantly lower ORR activation energy. The porous, rough morphology of CM3, driven by the synergistic combination of bio-Pd, activated charcoal, and carbon black, likely facilitates oxygen diffusion and electron transfer, key factors in ORR efficiency. Carbon black's high conductivity and activated charcoal's large surface area complement bio-Pd's catalytic properties, likely creating an optimized microenvironment for ORR. Compared to platinum-based cathodes, which often suffer from biofouling and high costs, bio-Pd's microbial synthesis offers a sustainable, cost-effective alternative, aligning with the need for scalable MFC technologies.

These findings build on prior studies, such as Cheng *et al.*,<sup>15</sup> who demonstrated bio-Pd's efficacy on carbon nanotubes, but extend the application to air-cathode MFCs, an underexplored area. The uniform dispersion of bio-Pd in CM3, confirmed by EDS mapping, mitigates aggregation issues common in chemical Pd synthesis, enhancing long-term stability. However, limitations include the lack of surface area quantification (*e.g.*, BET analysis) and long-term durability data, which future



studies should address to fully elucidate bio-Pd's potential. Overall, the characterization data establish CM3 as a high-performance cathode, setting the stage for its superior power output in MFC experiments.

### 3.2 The effects of bio-Pd on MFC performance

The performance of four cathode types—CM1 (bio-Pd and activated charcoal powder, ACP), CM2 (ACP and carbon black), CM3 (bio-Pd, ACP, and carbon black), and CM4 (unmodified carbon mesh, control)—was evaluated in air-cathode microbial fuel cells (MFCs) to assess the impact of bio-palladium (bio-Pd) on power generation. Voltage, current density, and power density were measured across a range of external resistances (1–560 k $\Omega$ ) after 24 hours of operation, with experiments conducted in triplicate to ensure reproducibility. Voltage increased linearly with external resistance up to 27 k $\Omega$  for all cathodes, after which the rate of increase diminished (Fig. 3). CM3 consistently delivered the highest voltage, reaching a maximum of  $0.365 \pm 0.012$  V at 560 k $\Omega$ , followed by CM1 ( $0.310 \pm 0.009$  V), CM2 ( $0.275 \pm 0.011$  V), and CM4 ( $0.210 \pm 0.008$  V) (mean  $\pm$  SD,  $n = 3$ ). The superior voltage output of CM3 suggests enhanced oxygen reduction reaction (ORR) kinetics, likely due to the synergistic combination of bio-Pd's catalytic activity, carbon black's conductivity, and ACP's high surface area. Polarization curves (Fig. 4) showed a characteristic voltage drop with increasing current density,<sup>30</sup> reflecting activation, ohmic, and mass transfer losses.<sup>31</sup> CM3 exhibited the smallest voltage decline, maintaining 0.300 V at 12.3 mA m $^{-2}$  compared to CM1 (0.240 V), CM2 (0.200 V), and CM4 (0.150 V), indicating lower internal resistance and improved reaction kinetics. Power density curves (Fig. 5) revealed CM3's peak performance at  $3.70 \pm 0.15$  mW m $^{-2}$  (at 10.1 mA m $^{-2}$ ), significantly outperforming CM1 ( $0.60 \pm 0.04$  mW m $^{-2}$ ), CM2 ( $0.30 \pm 0.03$  mW m $^{-2}$ ), and CM4 ( $0.08 \pm 0.01$  mW m $^{-2}$ ). CM3's broader power density curve suggests operational flexibility across a wide current density

range, a critical factor for practical MFC applications. Maximum power density calculated using the open-circuit voltage (OCV) and internal resistance, further highlighted CM3's superiority at  $6.90 \pm 0.22$  mW m $^{-2}$ , followed by CM2 ( $1.60 \pm 0.09$  mW m $^{-2}$ ), CM1 ( $1.30 \pm 0.07$  mW m $^{-2}$ ), and CM4 ( $0.50 \pm 0.03$  mW m $^{-2}$ ) (Fig. 6). Internal resistance, derived from polarization curve slopes, was lowest for CM3 ( $210 \pm 15$   $\Omega$  m $^2$ ), compared to CM1 ( $340 \pm 20$   $\Omega$  m $^2$ ), CM2 ( $380 \pm 18$   $\Omega$  m $^2$ ), and CM4 ( $520 \pm 25$   $\Omega$  m $^2$ ). The reduced internal resistance in CM3 correlates with its enhanced conductivity and catalytic efficiency, minimizing ohmic losses.

The results demonstrate that bio-Pd significantly enhances MFC performance, with CM3 achieving a six-fold higher power density than the control (CM4). The incorporation of bio-Pd in CM1 and CM3 catalyses ORR by lowering activation energy, as bio-Pd nanoparticles (9.6–16.9 nm) provide abundant active sites for oxygen adsorption and dissociation, consistent with Quan *et al.*<sup>29</sup> CM3's superior performance stems from the synergistic interplay of bio-Pd, carbon black, and ACP. Carbon black's high electrical conductivity reduces ohmic losses,<sup>32</sup> while ACP's porous structure enhances oxygen accessibility,<sup>33</sup> as evidenced by CM3's lower internal resistance and sustained voltage at high current densities. In contrast, CM2, lacking bio-Pd, exhibited higher ohmic resistance, and CM4's minimal catalytic activity led to substantial activation and mass transfer losses, limiting its power output.

Interestingly, CM2 achieved a slightly higher maximum power (1.60 mW m $^{-2}$ ) than CM1 (1.30 mW m $^{-2}$ ), despite lower peak power density. This discrepancy may reflect CM2's lower ohmic resistance due to carbon black's conductivity, though its lack of bio-Pd restricts catalytic efficiency. The use of polyvinylidene fluoride (PVDF) as a binder in CM1–CM3 likely facilitated proton and electron transfer, with studies suggesting PVDF's stability surpasses traditional binders like Nafion.<sup>34</sup> Compared to platinum-based cathodes, which typically yield 10–20 mW m $^{-2}$  but suffer from high costs and biofouling, CM3's 3.70 mW m $^{-2}$  is competitive, especially given bio-Pd's sustainable synthesis and cost-effectiveness.

These findings build on prior work, such as Cheng *et al.*<sup>15</sup> who reported bio-Pd's efficacy on carbon nanotubes, but extend its application to air-cathode MFCs, an underexplored domain. The power density of CM3 (3.70 mW m $^{-2}$ ) surpasses many carbon-based cathodes (0.5–2.0 mW m $^{-2}$ ),<sup>4</sup> and approaches biocatalytic systems using enzymes (2–5 mW m $^{-2}$ ).<sup>10</sup> Compared to platinum-based systems, bio-palladium (bio-Pd) cathodes in microbial fuel cells (MFCs) present certain limitations that affect their practical application. First, in terms of longevity and durability, Although Pt cathodes generally provide superior catalytic activity for oxygen reduction reaction (ORR), bio-Pd cathodes demonstrate stable and gradually increasing voltage output in microbial fuel cells (MFCs), highlighting their durability under operational conditions. While their power densities remain lower than Pt, bio-Pd offers promising catalytic activity that can be further enhanced through optimization. Moreover, bio-Pd cathodes exhibit greater resistance to catalyst poisoning and biofouling, as the bacteria-derived catalyst layers possess self-regenerating properties and can better tolerate biofilm

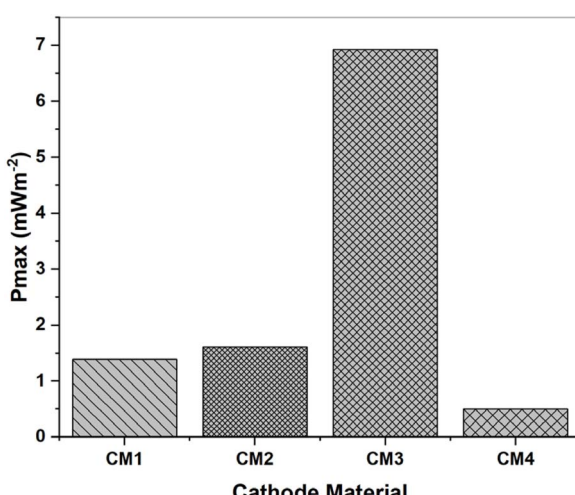


Fig. 6 The maximum power outputs of an air-cathode MFC using different cathode materials; CM1 – carbon mesh with bio-Pd and ACP, CM2 – carbon mesh with ACP and carbon black, CM3 – carbon mesh with bio-Pd, ACP and carbon black, and CM 4 carbon mesh.



formation, a factor that often diminishes Pt performance over time.<sup>14,35</sup> Secondly, regarding biofouling, both Pt and bio-Pd cathodes are susceptible to microbial colonization and biofilm accumulation, which may reduce the number of active catalytic sites,<sup>36</sup> however, bio-Pd nanoparticles promote the formation of biogenic Pd nanoparticle “shells” around bacterial cells, enhancing electron transfer and catalytic conductivity in cathode biofilms. This integration may reduce impedance and improve catalyst accessibility compared to Pt nanoparticles that tend to agglomerate.<sup>14</sup> Finally, with respect to scalability and cost, bio-Pd offers the advantages of lower material cost and environmentally friendly biosynthesis compared to the high expense and scarcity of Pt. Nevertheless, the catalytic activity and achievable power densities of bio-Pd cathodes typically remain below those of Pt under equivalent conditions, limiting their scalability for large-scale or commercial applications.<sup>14,37</sup> By contrast, platinum benefits from decades of industrial optimization, ensuring reliable, reproducible, and scalable cathode production, a benchmark that bio-Pd technologies are still working to achieve. Future studies should explore bio-Pd's durability, scalability, stability long-term and integration with advanced anode materials to further enhance MFC performance. Previous work has shown that bio-Pd nanoparticles, while catalytically active, may undergo leaching, or surface poisoning over time, leading to gradual loss of activity.<sup>14</sup> Furthermore, biofouling by non-electrogenic microbes can accelerate catalyst deactivation.<sup>38</sup> Although our study was limited to batch-scale tests, we acknowledge the need for extended operation studies under realistic conditions (weeks to months) to evaluate bio-Pd stability. Future work will employ continuous-flow MFCs and monitor catalyst structural integrity. These results underscore bio-Pd's potential as a sustainable cathode catalyst, advancing MFC technology toward practical applications in wastewater treatment and renewable energy generation.

### 3.3 The effect of microbial culture on MFC performance

**3.3.1 Comparison of MFC performance between SRB and MB.** To investigate the influence of microbial consortia on MFC performance, the CM3 cathode (0.3 g activated charcoal powder, 0.03 g carbon black, 6 mg bio-Pd) was paired with two microbial cultures: sulfate-reducing bacteria (SRB) and marine bacteria (MB). Experiments were conducted in triplicate over 48 hours, with voltage, current density, and power density measured across external resistances (1–560 kΩ) to assess bioelectricity generation.

Voltage increased linearly with resistance up to 27 kΩ, then plateaued (Fig. 7). The MB culture consistently outperformed SRB, achieving a maximum voltage of  $0.315 \pm 0.010$  V at 560 kΩ, compared to  $0.310 \pm 0.009$  V for SRB. This slight voltage advantage suggests MB's superior electron transfer efficiency, potentially due to its microbial composition and adaptation to the mineral salt medium (MSM).<sup>39</sup> This trend is also reflected in Fig. 8, where increasing bacterial growth corresponded with rising voltage output.<sup>40</sup> Notably, during the first 8 hours of incubation, voltage decreased despite continued bacterial

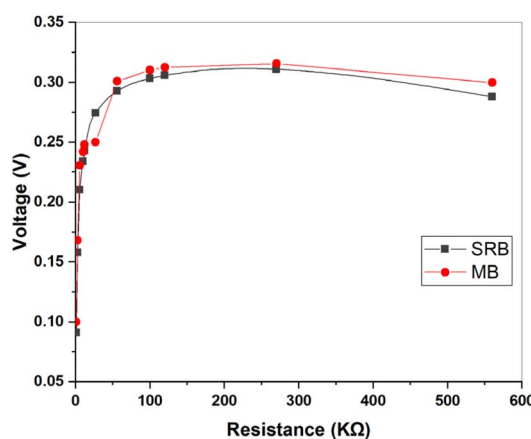


Fig. 7 Voltage vs. resistance curves for MFC inoculated with sulfate-reducing bacteria (SRB) and marine bacteria (MB).

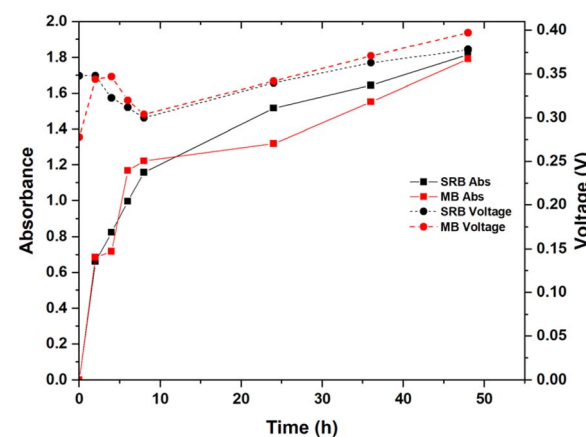


Fig. 8 Relationship between bacterial growth ( $OD_{600}$ ) and voltage generation in MFCs inoculated with sulfate-reducing bacteria (SRB) and marine bacteria (MB). Both cultures show a positive correlation between growth and voltage over time.

growth in both cultures. This initial decline may have been attributed to frequent sampling, which could have disturbed the system's stability, as well as possible lag-phase metabolic adjustments or incomplete biofilm attachment to the electrode surface.<sup>41</sup> From 8 hours onwards, voltage increased steadily, with MB maintaining slightly higher values than SRB, even though SRB exhibited marginally greater bacterial growth. These observations are consistent with SEM analyses presented in Section 3.3.3, which showed denser and more uniform biofilm coverage on the MB anode. Such extensive biofilm formation likely enhanced direct electron transfer, thereby contributing to MB's increased voltage output and overall MFC performance.

Polarization curves (Fig. 9A) revealed that MB maintained higher voltages across a broad current density range, with a minimal drop to 0.280 V at  $14.2 \text{ mA m}^{-2}$ , compared to SRB's 0.260 V at  $13.8 \text{ mA m}^{-2}$ . Power density curves (Fig. 9B) confirmed MB's superior performance, peaking at  $4.18 \pm 0.17 \text{ mW m}^{-2}$  (at  $11.5 \text{ mA m}^{-2}$ ), significantly higher than SRB's  $3.69 \pm 0.14 \text{ mW m}^{-2}$ .



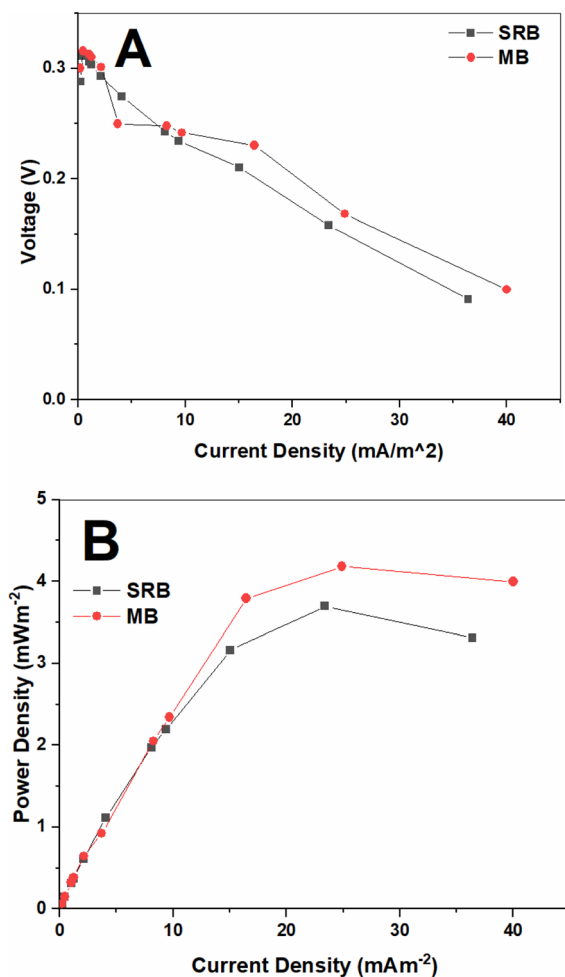


Fig. 9 (A) Polarisation curves and (B) power density curves for MFC inoculated with SRB and MB. The data highlights the influence of microbial communities on the electrochemical behaviour of MFCs.

$\text{m}^{-2}$ . MB's broader power density curve indicates greater operational stability, critical for practical MFC applications. Internal resistance, derived from polarization slopes, was lower for MB ( $190 \pm 12 \Omega \text{ m}^2$ ) than SRB ( $220 \pm 15 \Omega \text{ m}^2$ ), reflecting reduced ohmic losses and enhanced electron transfer kinetics. MB's enhanced performance is attributed to its adaptation to MSM's higher ionic strength ( $\sim 20 \text{ mS cm}^{-1}$ ), which facilitates ion transport and reduces ohmic resistance, as noted by Liu *et al.*<sup>42</sup> Estuarine MB, likely moderate halophiles tolerant to 0.8–3.4 M NaCl, thrive in MSM's saline conditions,<sup>43</sup> unlike SRB, which may face salinity-induced activation losses in Postgate Medium C. Additionally, MB's dense biofilm formation (Section 3.3.3) enhances direct electron transfer, contributing to higher power output. The MB-driven MFC's power density ( $4.18 \text{ mW m}^{-2}$ ) surpasses many SRB-based systems ( $1\text{--}3 \text{ mW m}^{-2}$ )<sup>44</sup> and approaches bio-catalytic MFCs using *Geobacter sulfurreducens* ( $4\text{--}6 \text{ mW m}^{-2}$ ).<sup>45</sup> Matsena *et al.*<sup>16</sup> reported the maximum power density of approximately  $4.01 \text{ mW m}^{-2}$  using bio-Pd nanoparticles and *Citrobacter* sp. to enhance anode electrocatalytic activity. In comparison, microbe-only catalytic microfluidic fuel cells generally exhibit lower power densities, often around  $10^{-4}$

$\text{mW cm}^{-2}$  or less at the electrode level, with some improved designs reaching  $\sim 0.012 \text{ mW cm}^{-2}$  (ref. 46) and up to  $54 \text{ mW m}^{-2}$ .<sup>47</sup> Although bio-Pd cathodes currently produce lower peak power densities than optimized Pt and Pd nanomaterial systems, they offer distinct advantages in terms of cost, sustainability, and environmentally friendly synthesis, making them a promising and scalable catalyst option for future microbial fuel cell development.

### 3.3.2 Microbial culture characterisation for SRB and MB.

Metagenomic analysis of 16S rRNA gene amplicons revealed distinct microbial compositions. The SRB culture was dominated by *Escherichia* (83%), with *Desulfovibrio* (13%) and unidentified taxa (4%) (Fig. 10). *Desulfovibrio* is a known electrogene, capable of direct extracellular electron transfer via c-type cytochromes.<sup>44</sup> While *Escherichia coli* is typically non-electrogenic,<sup>33,44</sup> recent studies<sup>48</sup> suggest it can contribute to electron transfer in mixed consortia, though its dominance may limit SRB's overall efficiency. According to Logan *et al.*<sup>49</sup> the presence of non-electrogenic bacteria such as *Escherichia coli* within the SRB could act as a metabolic sink, competing for substrates without contributing effectively to extracellular electron transfer. Such species may reduce the overall electron recovery efficiency, thereby lowering the MFC performance relative to the MB consortia. A similar finding was reported in mixed-culture MFCs where non-electrogenic bacteria diluted the electroactive community fraction.<sup>50</sup> In contrast, the MB culture consisted entirely of *Paraclostridium* sp. (100%), a newly identified electroactive bacterium.<sup>51</sup> *Paraclostridium*'s ability to form conductive biofilms and utilize both direct and mediated electron transfer pathways likely drives MB's superior performance.

Recent studies indicate that certain *Paraclostridium* species initiate anode colonization through physicochemical interactions and microbial adhesins that mediate surface attachment, followed by the secretion of extracellular polymeric substances (EPS) that form a protective, adhesive matrix that promotes dense biofilm development, enabling close cell packing and retention of redox mediators. Biofilm formation enhances electron transfer efficiency by maintaining direct or mediated

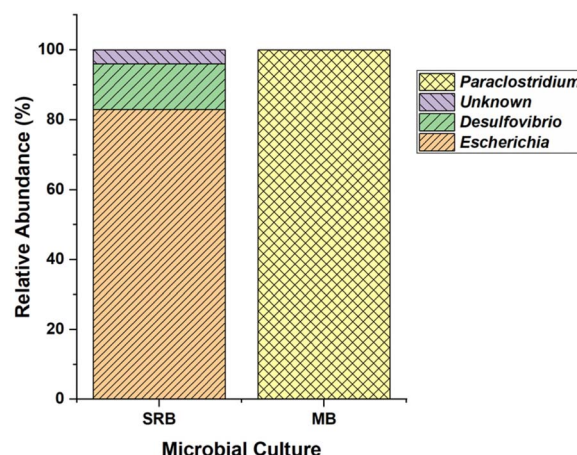


Fig. 10 16s rRNA analysis of SRB and MB.



contact between cells and the electrode.<sup>51,52</sup> Direct electron transfer involves the microbe forming a direct physical connection with the electrode, such as through biofilms or conductive structures like nanowires and flagella.<sup>51</sup> Indirect transfer utilizes electron mediators. Although *Paraclostridium* lacks the typical outer membrane cytochromes found in classical Gram-negative electrogenergs, it achieves indirect electron transfer through soluble redox mediators such as flavins (e.g., riboflavin and flavin adenine dinucleotide) that it secretes into the extracellular environment. These electron shuttles diffuse between the cells and electrode, facilitating electron transfer over distances greater than direct contact allows. Addition of flavins significantly boosts current, confirming this mediated pathway.<sup>53</sup> Scanning electron microscopy (SEM) of anode surfaces revealed significant differences in biofilm formation. MB formed a dense, uniform biofilm with interconnected microbial clusters, indicating robust attachment and high electroactive cell density (Fig. 11B). SRB, however, exhibited a sparser biofilm with fewer cells, suggesting limited anode colonization (Fig. 11C). These observations align with MB's higher power output, as denser biofilms reduce electron transfer resistance, as reported by Hu *et al.*<sup>45</sup> The microbial characterization explains MB's enhanced MFC performance. *Paraclostridium*'s electroactive properties, including biofilm formation and versatile electron transfer mechanisms, outperform the SRB consortium, where *Escherichia*'s dominance may dilute *Desulfovibrio*'s contribution. The unidentified 4% in SRB introduces potential variability, warranting further taxonomic analysis. Compared to literature, *Paraclostridium*'s performance ( $4.18 \text{ mW m}^{-2}$ ) is notable, though lower than its reported maximum ( $393 \text{ mW m}^{-2}$ ) in optimized conditions,<sup>51</sup> likely due to differences in electrolyte or anode design. Future studies should explore MB's metabolic pathways and synergy with bio-

Pd to further enhance power output, while long-term biofilm stability, quantification and scalability remain critical areas for investigation.

**3.3.3 Microbial electron transfer at the MFC anode.** The efficiency of electron transfer from microbial cells to the anode surface is a critical determinant of MFC performance, mediated by direct electron transfer (DET) *via* membrane-bound redox proteins or indirect electron transfer (IET) through electron shuttles (Fig. 12). The superior power density of the marine bacteria (MB) culture ( $4.18 \pm 0.17 \text{ mW m}^{-2}$ ) compared to sulfate-reducing bacteria (SRB) ( $3.69 \pm 0.14 \text{ mW m}^{-2}$ ) suggests MB possesses more effective electron transfer mechanisms. Metagenomic analysis identified MB as entirely *Paraclostridium* sp., a recently recognized electroactive bacterium, while SRB comprised *Escherichia* (83%), *Desulfovibrio* (13%), and unidentified taxa (4%).

*Paraclostridium*'s electrochemical activity, as reported by Basu *et al.*,<sup>51</sup> involves both DET through conductive biofilms and IET *via* secreted redox mediators, enabling efficient electron transfer to the anode. Scanning electron microscopy (SEM) revealed MB's dense, interconnected biofilm on the anode, with a surface coverage of approximately 85% (Fig. 11B), facilitating DET by minimizing electron transfer resistance. In contrast, SRB's sparser biofilm (coverage  $\sim 40\%$ , Fig. 11C) suggests fewer electroactive cells, likely dominated by non-electrogenic *Escherichia*, which limits DET efficiency. *Desulfovibrio*, known for DET *via* c-type cytochromes,<sup>44</sup> is underrepresented in SRB, reducing its contribution. The role of anode materials is also central to these differences. Carbon-based anodes, as highlighted by Fan *et al.*<sup>54</sup> strongly influence both microbial attachment and extracellular electron transfer (EET). Porous three-dimensional carbon structures, such as the granulated carbon used in this study (Fig. 11A), provide a high surface area

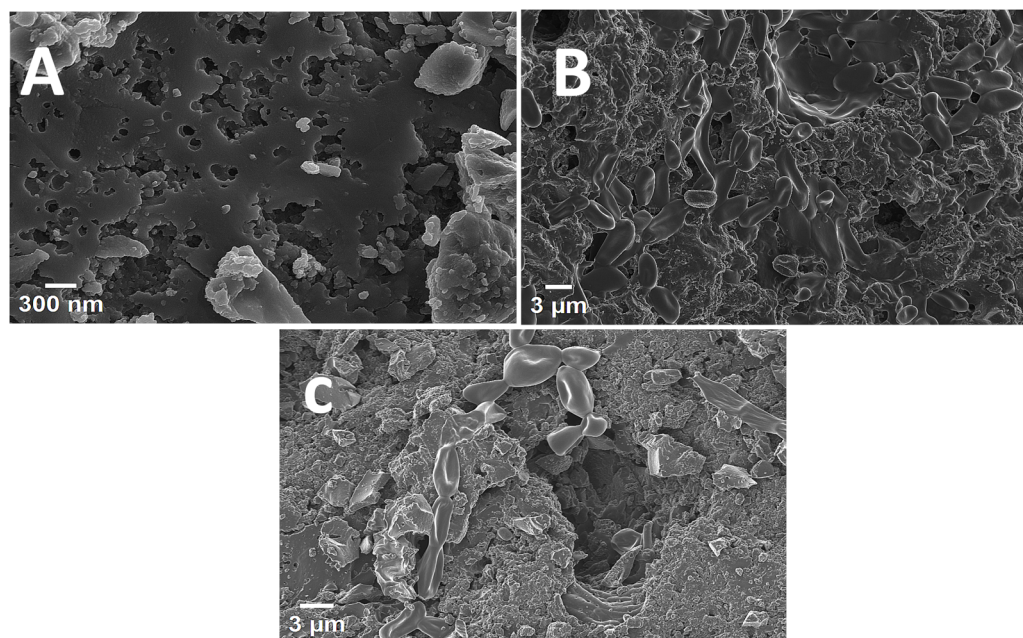


Fig. 11 SEM analysis depicting (A) the surface of the anode, (B) MB attachment to the anode and (C) SRB attachment to the anode.



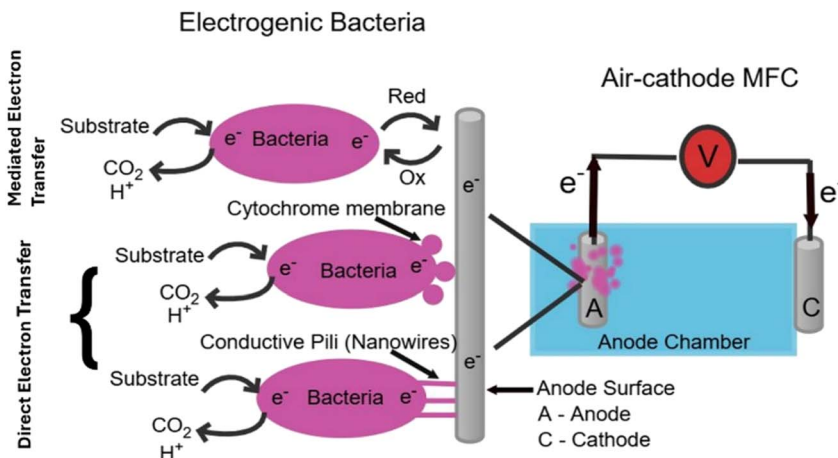


Fig. 12 Electron transfer mechanism at the anode – microbes transfer electrons through two main processes: direct electron transfer and indirect transfer. Direct electron transfer involves the microbe forming a direct physical connection with the electrode, such as through biofilms or conductive structures like nanowires and flagella. Indirect transfer utilizes electron mediators.

and internal colonization sites that promote bacterial adhesion and mass transfer. MB benefitted significantly from this architecture, forming thick and uniform biofilms (estimated at  $10\text{--}15\ \mu\text{m}$  via SEM) that enabled more efficient DET, whereas SRB showed weaker attachment. This is consistent with findings that 3D porous carbon anodes enhance biofilm formation, reduce internal resistance, and improve conductivity compared to planar materials. MB's lower internal resistance ( $190 \pm 12\ \Omega\text{ m}^2$  vs. SRB's  $220 \pm 15\ \Omega\text{ m}^2$ ) correlates with its robust biofilm structure and efficient electron transfer, supporting higher current density ( $11.5\ \text{mA m}^{-2}$  vs.  $10.8\ \text{mA m}^{-2}$ ). A low internal resistance is key in achieving long term stability, it improves current collection and minimizes voltage losses, ensuring consistently higher power output over time. It also promotes uniform biofilm growth during startup, which enhances microbial activity and maximizes power density.<sup>55</sup> By reducing energy losses and heat generation, system components such as electrodes and membranes are protected from thermal stress, extending their durability. In addition, lower resistance decreases mass-transfer limitations, allowing more efficient substrate delivery and product removal, which strengthens microbial electrochemical reactions.<sup>56</sup> Importantly, MFCs with reduced internal resistance remain stable under varying conditions, such as changes in substrate concentration or retention time. Together, these benefits translate into more reliable, efficient, and long-lasting MFC performance in practical applications.<sup>55</sup> In addition, *Paraclostridium*'s potential to form conductive nanowires, as hypothesized by Basu *et al.*<sup>51</sup> may further enhance DET, although nanowire presence was not confirmed in this study. SRB's performance likely relies on IET *via* flavins or other shuttles, which is less efficient at high current densities due to diffusion limitations, as noted by Kumar *et al.*<sup>57</sup>

*Paraclostridium*'s power density ( $4.18\ \text{mW m}^{-2}$ ) is competitive with *Geobacter sulfurreducens* ( $4\text{--}6\ \text{mW m}^{-2}$ ),<sup>45</sup> a model exoelectrogen, but lower than its reported maximum ( $393\ \text{mW m}^{-2}$ )<sup>51</sup> in optimized conditions, suggesting potential for further

enhancement. Unlike *Geobacter*'s thick biofilms and nanowires, *Paraclostridium*'s versatility in DET and IET offers adaptability to varying anode conditions. SRB's performance, driven by *Desulfovibrio*, is comparable to mixed consortia ( $1\text{--}3\ \text{mW m}^{-2}$ )<sup>44</sup> but limited by *Escherichia*'s non-electrogenic dominance. Studies on *Escherichia*<sup>48</sup> indicate minimal DET, reinforcing its secondary role in SRB.

## 4 Conclusions

This study advances air-cathode microbial fuel cell (MFC) performance by integrating bio-palladium (bio-Pd) catalysts and optimized microbial consortia. The CM3 cathode, combining bio-Pd, activated charcoal, and carbon black, achieved a peak power density of  $3.70 \pm 0.15\ \text{mW m}^{-2}$  six times higher than the control, driven by bio-Pd's nanoscale size (9.6–16.9 nm) and low internal resistance ( $210 \pm 15\ \Omega\text{ m}^2$ ). The marine bacteria (MB) culture, dominated by electroactive *Paraclostridium* sp., outperformed sulfate-reducing bacteria (SRB), delivering  $4.18 \pm 0.17\ \text{mW m}^{-2}$  due to its dense biofilm (85% anode coverage) and efficient electron transfer mechanisms. These findings position bio-Pd as a sustainable potential catalyst and highlight's *Paraclostridium*'s potential as a high-performance inoculum. Addressing South Africa's energy challenges and aligning with UN Sustainable Development Goals (6, 7, 9, 13), this work supports clean energy and wastewater treatment applications. Limitations include modest power density compared to platinum-based systems and short-term (48 hours) data. Future research should explore bio-Pd's long-term stability, *Paraclostridium*'s electron transfer pathways, and scalability for industrial applications. These advancements pave the way for cost-effective, sustainable MFCs with global relevance.

## Author contributions

Khanyisile B. Malunga-Makatu: conceptualisation, methodology, formal analysis, investigation, writing – original draft,



writing- review & editing, visualisation. Evans M. N. Chirwa: methodology, validation, investigation, resources, writing – review & editing, supervision. Shepherd M. Tichapondwa: writing – review & editing, supervision.

## Conflicts of interest

The authors declare that they have no known competing financial interests or personal relationships that could have appeared to influence the work reported in this paper.

## Data availability

The data supporting the findings of this study are available within the article. Data presented in the figures in the main manuscript can be accessed directly from the publication.

## Acknowledgements

The authors would like to thank the Water Utilisation and Environmental Engineering Division of the University of Pretoria for the financial support during the study. This research was funded by the National Research Fund (NRF) through the grant number: MND210623615156 awarded to Khanyisile Malunga-Makatu and grant number: SRUG2204072544 awarded to Prof Evans Chirwa of the Department of Chemical Engineering and auxiliary items financed by the Rand Water Chair in Water Utilisation grant no. RW01413/18 awarded to Professor Evans M. N. Chirwa of the University of Pretoria (South Africa).

## References

- 1 M. A. Costa de Oliveira, A. D'Epifanio, H. Ohnuki and B. Mecheri, *Catalysts*, 2020, **10**, 475.
- 2 M. Nhleko and F. Inambao, *Int. J. Eng. Res. Sci. Technol.*, 2020, **13**, 2814.
- 3 A. Resolution, Seventieth United Nations General Assembly, New York, 2015, vol. 25, pp. 86–97.
- 4 R. Chakma, M. K. Hossain, P. Paramasivam, R. Bousbih, M. Amami, G. F. I. Toki, R. Haldhar and A. K. Karmaker, *Global Chall.*, 2025, **9**(5), 250004.
- 5 C. Santoro, C. Arbizzani, B. Erable and I. Ieropoulos, *J. Power Sources*, 2017, **356**, 225–244.
- 6 J. Wang, K. Ren, Y. Zhu, J. Huang and S. Liu, *BioTech*, 2022, **11**(4), 44.
- 7 A. A. Yaqoob, A. Khatoon, S. H. Mohd Setapar, K. Umar, T. Parveen, M. N. Mohamad Ibrahim, A. Ahmad and M. Rafatullah, *Catalysts*, 2020, **10**(8), 819.
- 8 A. Y. Ganaraja and L. Mulky, *Environ. Technol. Rev.*, 2024, **13**, 235–250.
- 9 V. Gadhamshetty, D. Belanger, C.-J. Gardiner, A. Cummings and A. Hynes, *Bioresour. Technol.*, 2013, **127**, 378–385.
- 10 S. Qiu, Z. Guo, F. Naz, Z. Yang and C. Yu, *Bioelectrochemistry*, 2021, **141**, 107834.
- 11 Y. Yuan, T. Yuan, D. Wang, J. Tang and S. Zhou, *Bioresour. Technol.*, 2013, **144**, 115–120.
- 12 Ø. Hasvold, H. Henriksen, E. Melvear, G. Citi, B. Ø. Johansen, T. Kjønigsen and R. Galetti, *J. Power Sources*, 1997, **65**, 253–261.
- 13 K. S. Siddiqi and A. Husen, *Nanoscale Res. Lett.*, 2016, **11**, 482.
- 14 A. J. Stephen, N. V. Rees, I. Mikheenko and L. E. Macaskie, *Front. Energy Res.*, 2019, **7**, 66.
- 15 H.-Y. Cheng, Y.-N. Hou, X. Zhang, Z.-N. Yang, T. Xu and A.-J. Wang, *Sci. Rep.*, 2017, **7**, 16588.
- 16 M. T. Matsena, S. M. Tichapondwa and E. M. N. Chirwa, *Catalysts*, 2020, **10**, 838.
- 17 R. Gobalakrishnan and R. Bhuvaneswari, *Biotechnol. Res. Innov.*, 2019, **3**, 144–158.
- 18 M. Alemán-Vega, I. Sánchez-Lozano, C. A.-O. Hernández-Guerrero, C. A.-O. Hellio and E. T. Quintana, *Int. J. Mol. Sci.*, 2020, **21**(17), 6068.
- 19 C. Li, Y. Xie, J. Wang, C. Guo, L. Han, Z. Xia, Z. Zhang, J. Wang, M. Li, W. Han, L. Huang, J. Yan and H. Zhang, *Environ. Res.*, 2025, **279**, 121857.
- 20 M. I. Pérez-Díaz, P. Zárate-Segura, L. A. Bermeo-Fernández, K. Nirmalkar, F. Bastida-González, J. García-Mena, J. Jan-Roblero and C. Guerrero-Barajas, *J. Environ. Health Sci. Eng.*, 2020, **18**, 1189–1205.
- 21 K. B. Malunga and E. Chirwa, *Chem. Eng. J.*, 2019, **74**, 1519–1524.
- 22 P. E. Molokwane and E. M. Nkhalambayaus-Chirwa, *Water Sci. Technol.*, 2009, **60**, 381–388.
- 23 M. Van der Velden, M. T. Matsena and E. Chirwa, *Chem. Eng. J.*, 2022, **96**, 331–336.
- 24 B. E. Logan, Power Generation, *Microbial Fuel Cells*, John Wiley & Sons, 1st edn, 2008, pp. 44–57.
- 25 P. Yong, N. A. Rowson, J. P. G. Farr, I. R. Harris and L. E. Macaskie, *Biotechnol. Bioeng.*, 2002, **80**, 369–379.
- 26 M. D. Redwood, K. Deplanche, V. S. Baxter-Plant and L. E. Macaskie, *Biotechnol. Bioeng.*, 2008, **99**, 1045–1054.
- 27 G. A. Somorjai and R. M. Rioux, *Catal. Today*, 2005, **100**, 201–215.
- 28 X. Zhang, X. Xia, I. Ivanov, X. Huang and B. E. Logan, *Environ. Sci. Technol.*, 2014, **48**(3), 2075–2081.
- 29 X. Quan, Y. Mei, H. Xu, B. Sun and X. Zhang, *Electrochim. Acta*, 2015, **165**, 72–77.
- 30 J. Guo, J. Cheng, J. Wang, Z. Zhang, X. Xie and P. Chu, *Water Sci. Technol.*, 2020, **81**, 1972–1982.
- 31 F. Valle, PhD dissertation, Università degli Studi di Trieste, 2015.
- 32 J. Zhang, *PEM Fuel Cell Electrocatalysts and Catalyst Layers: Fundamentals and Applications*, Springer Science & Business Media, 2008.
- 33 T. Niu, *Nano Today*, 2018, **18**, 12–14.
- 34 Y. Yang, C. Choi, G. Xie, J.-D. Park, S. Ke, J.-S. Yu, J. Zhou and B. Lim, *Bioelectrochemistry*, 2019, **127**, 94–103.
- 35 H.-L. Song, Y. Zhu and J. Li, *Arabian J. Chem.*, 2019, **12**(8), 2236–2243.
- 36 M. Kodali, S. Herrera, S. Kabir, A. Serov, C. Santoro, I. Ieropoulos and P. Atanassov, *Electrochim. Acta*, 2018, **256**, 56–64.



37 S. Baskar, J. Jayaprabakar, R. A, T. S. Rajan, J. A. Kumar, N. R. U, B. E, P. Sambandam, J. Pk and M. Ruban, *Results Eng.*, 2025, **25**, 104161.

38 O. O. Kolajo, C. Pandit, B. S. Thapa, S. Pandit, A. S. Mathuriya, P. K. Gupta, D. A. Jadhav, D. Lahiri, M. Nag and V. J. Upadhye, *Biocatal. Agric. Biotechnol.*, 2022, **43**, 102408.

39 M. Grattieri and S. D. Minteer, *Bioelectrochemistry*, 2018, **120**, 127–137.

40 S.-S. Wu, M. Hernández, Y.-C. Deng, C. Han, X. Hong, J. Xu, W.-H. Zhong and H. Deng, *FEMS Microbiol. Ecol.*, 2019, **95**, fiz018.

41 C. Ihenacho, C. Akujobi, H. Anuforo and C. Nwaneri, *GSC Adv. Res. Rev.*, 2023, **16**, 38–49.

42 G. Liu, M. D. Yates, S. Cheng, D. F. Call, D. Sun and B. E. Logan, *Bioresour. Technol.*, 2011, **102**, 7301–7306.

43 M. Dopson, G. Ni and T. H. Sleutels, *FEMS Microbiol. Rev.*, 2016, **40**, 164–181.

44 C. S. Kang, N. Eaktasang, D.-Y. Kwon and H. S. Kim, *Bioresour. Technol.*, 2014, **165**, 27–30.

45 Y. Hu, Y. Wang, X. Han, Y. Shan, F. Li and L. Shi, *Front. Bioeng. Biotechnol.*, 2021, **9**, 786416.

46 J. W. Lee and E. Kjeang, *Biomicrofluidics*, 2010, **4**, 041301.

47 S. V. Ramanaiah, C. M. Cordas, S. C. Matias, M. V. Reddy, J. H. Leitão and L. P. Fonseca, *Biotechnol. Rep.*, 2021, **32**, e00693.

48 C. Montoya-Vallejo, J. O. Gil Posada and J. C. Quintero-Díaz, *Energies*, 2023, **16**, 7901.

49 B. Logan, R. Rossi, A. Ragab and P. Saikaly, *Nat. Rev. Microbiol.*, 2019, **17**, 1.

50 S. Ishii, S. Suzuki, Y. Yamanaka, A. Wu, K. H. Nealson and O. Bretschger, *Bioelectrochemistry*, 2017, **117**, 74–82.

51 A. Basu, S. Manna and A. Kumar Sil, *Chem. Eng. J.*, 2023, **475**, 145626.

52 K. Yanuka-Golub, V. Dubinsky, E. Korenblum, L. Reshef, M. Ofek-Lalzar, J. Rishpon and U. Gophna, *mBio*, 2021, **12**(2), 3629.

53 J. J. M. Lustermans, N. Basu, L. Digel and K. Aiyer, *bioRxiv*, 2025, preprint, DOI: [10.1101/2024.09.12.612730](https://doi.org/10.1101/2024.09.12.612730).

54 X. Fan, Y. Zhou, X. Jin, R. B. Song, Z. Li and Q. Zhang, *Carbon Energy*, 2021, **3**, 449–472.

55 Y. Fan, A. Janicek and H. Liu, *Eur. Chem. Biotechnol. J.*, 2024, 47–57.

56 R. Rossi and B. E. Logan, *Electrochim. Acta*, 2020, **348**, 136291.

57 S. S. Kumar, V. Kumar, V. Gnaneswar Gude, S. K. Malyan and A. Pugazhendhi, *Bioresour. Technol.*, 2020, **306**, 123110.

